One-step theory of photoelectron escape time: Attosecond spectroscopy of Mg(0001)

R. O. Kuzian [1,2] and E. E. Krasovskii [2,3,4]

[1]*Institute for Problems of Materials Science NASU, Krzhizhanovskogo 3, 03180 Kiev, Ukraine*
[2]*Donostia International Physics Center (DIPC), Paseo Manuel de Lardizabal 4, San Sebastián/Donostia, 20018 Basque Country, Spain*
[3]*Departamento de Física de Materiales, Facultad de Ciencias Químicas, Universidad del Pais Vasco/Euskal Herriko Unibertsitatea, Apdo. 1072, San Sebastián/Donostia, 20080 Basque Country, Spain*
[4]*IKERBASQUE, Basque Foundation for Science, 48013 Bilbao, Spain*

A theory of photoelectron escape time τ from crystals is presented that combines the one-step photoemission theory with the Wigner delay. Equations are formally derived and illustrated with an exactly solvable model. An *ab initio* implementation with the augmented-plane-wave-based scattering method is applied to emission from Mg(0001). The theory is in reasonable agreement with streaking measurements. Lattice scattering is found to cause rapid variations of τ with photon energy both for the valence band and for the $2p$ core band emission, and a strong dependence on the initial state is revealed.

I. INTRODUCTION

Recent experimental progress in time-resolved photoemission from solids [1–10] calls for a theory that fully allows for three-dimensional (3D) multiple scattering and its implications for photoelectron escape time—the key parameter in both streaking spectroscopy [1–7,11–13] and RABBITT interferometry [8–10,14,15]. Solid-state photoemission is fundamentally different from the well-studied isolated-atom problem [16–18]: In the crystal, initial states are infinitely extended and the propagation of the outgoing electron is limited by inelastic scattering, so the photoelectron "starting point" depends on its mean-free path (MFP). Theoretical approaches to attosecond photoemission from crystals until now have been restricted to one-dimensional (1D) models [7,11–15,19–23], also heuristically combined with isolated-atom calculations [5]. Measured delays are commonly interpreted (at least partially) in terms of an effective escape depth and velocity with which the photoelectron travels to reach the probe-field area [1–15,22,24,25]. The semiclassical kinematics is, however, not applicable when the photoemission final state lies in a band gap [26] or, more generally, when the final state has a strong contribution from evanescent waves, which cannot be ascribed a group velocity. Furthermore, in 3D crystals, more than one propagating wave may contribute to the final state [27]. Generally, the singularity of the atomic potential and the multiple scattering by the 3D lattice make a phenomenological inclusion of the band structure rather unreliable and, at the same time, the time-dependent Schrödinger equation (TDSE) becomes computationally forbidding. An alternative is offered by the one-step theory [28–32], in which the photoexcitation and escape are embodied in the time-reversed LEED (low-energy electron diffraction) state Φ^*. The wave function Φ^* treats on the same footing propagating and evanescent Bloch states and naturally allows for inelastic scattering via the imaginary optical potential $-iV_i$ [33,34]. Here, we present an *ab initio* theory that combines the classical one-step theory

with the Eisenbud-Wigner-Smith (EWS) phase delay formalism [35–37]. The one-step approach is standard in stationary photoemission and was applied to pump-probe spectroscopy in Refs. [38,39], but the escape time was not addressed there.

II. THEORY

Consider a semi-infinite crystal irradiated by a short extreme ultraviolet (XUV) pulse with a vector potential

$$\mathbf{A}(\mathbf{x}, t) = \alpha(t)\mathbf{A}(\mathbf{x}), \quad \text{where } \alpha(t) \equiv F(t)\cos\omega_{\mathrm{x}}t. \quad (1)$$

The envelope function $F(t)$ vanishes outside a subfemtosecond time interval. Far from the sample, the time-dependent density of photoelectrons $n(\mathbf{X}, t)$ is an incoherent superposition of wave packets coming from all initial states ψ_i. The crest of the wave packet reaches the detector at $\mathbf{X}$ at a time $t = X/v + \tau_i$ relative to the maximum of $F(t)$, where v is the group velocity in vacuum and τ_i is the intercept time we are interested in.

In the theory of photoemission from atoms [16–18], the intercept τ_i is related to the EWS scattering delay given by the energy derivative of the scattering phase $\tau = d\eta/dE$ [35–37], and in certain cases τ_i simply equals half of the EWS delay [18]. In contrast to the isolated atom, the photoemission from a semi-infinite crystal cannot be immediately mapped onto a physical scattering process: First, the unperturbed wave does not have the same asymptotics as the scattered wave because the free motion is restricted to the vacuum half-space. Second, the probability current is not conserved: photoelectrons are absorbed in the interior of the crystal, which makes solid-state photoemission surface-sensitive.

To formally derive the expression for τ_i for crystals, let us calculate the "lesser" Green's function (GF)

$$G^+(\mathbf{x}, t, \mathbf{x}', t') = i\langle\hat{\psi}^\dagger(\mathbf{x}', t')\hat{\psi}(\mathbf{x}, t)\rangle \quad (2)$$

[30,40] to the second order of the electron-light coupling $\hat{O}(\mathbf{x}, t)$. The angular brackets denote the thermodynamic average with the *equilibrium* density matrix: $\langle \hat{A} \rangle \equiv \text{Tr}[\exp(-\beta \hat{H}_0)\hat{A}]/\text{Tr}[\exp(-\beta \hat{H}_0)]$, where β is the inverse temperature. The operator $\hat{\psi}(\mathbf{x})$ annihilates an electron at point $\mathbf{x}$, and its time dependence is governed by the full Hamiltonian

$$\hat{H}(\mathbf{x}, t) = \hat{H}_0(\mathbf{x}) + \hat{O}(\mathbf{x}, t), \tag{3}$$

$$\hat{O}(\mathbf{x}, t) = \alpha(t)\hat{a}(\mathbf{x}), \tag{4}$$

$$\hat{a}(\mathbf{x}) = -\frac{i}{c}[\mathbf{A}(\mathbf{x}) \cdot \nabla + \nabla \cdot \mathbf{A}(\mathbf{x})]. \tag{5}$$

The time-dependent density of excited electrons is expressed via GF [40]:

$$n(\mathbf{X}, t) = \lim_{\mathbf{X}' \to \mathbf{X} \to \infty} -iG_2^+(\mathbf{X}, t, \mathbf{X}', t). \tag{6}$$

The second-order GF G_2^+ is calculated from the Dyson equation for the Keldysh contour-ordered GF $G(\mathbf{x}, t, \mathbf{x}', t') = -i\langle T_C \hat{\psi}(\mathbf{x}, t)\hat{\psi}^\dagger(\mathbf{x}', t')\rangle$ [30,40,41], see Appendix A. Following the perturbation theory of Ref. [30], for the case of a ground state bound to the crystal half-space and all the excited electrons being unbound, we obtain (in units $\hbar = e = m_e = 1$):

$$G_2^+(\mathbf{X}, t, \mathbf{X}', t) = \iint d^3\mathbf{x}_2 d^3\mathbf{x}_3 \iiint \frac{d\epsilon \, d\epsilon' dE}{8\pi^3} G_0^r(\mathbf{X}, \mathbf{x}_2, \epsilon)\hat{o}(\mathbf{x}_2, \epsilon - \omega_X - E)$$

$$\times G_0^+(\mathbf{x}_2, \mathbf{x}_3, E)\,\hat{o}(\mathbf{x}_3, E + \omega_X - \epsilon')G_0^a(\mathbf{x}_3, \mathbf{X}', \epsilon')\exp[i(\epsilon' - \epsilon)t],$$

$$\text{where } G_0^r(\mathbf{x}_1, \mathbf{x}_2, \epsilon) = -i\int_0^\infty \langle\{\hat{\psi}(\mathbf{x}_1, t), \hat{\psi}^\dagger(\mathbf{x}_2, 0)\}\rangle \exp(i\epsilon t)\,dt, \quad \hat{o}(\mathbf{x}, \omega) \equiv \frac{1}{2}F(\omega)\hat{a}(\mathbf{x}), \quad F(\omega) \equiv \int_{-\infty}^{+\infty} F(t)e^{i\omega t}\,dt. \tag{7}$$

In Eq. (7), G_0^r and G_0^a are the equilibrium retarded and advanced GFs. The substitution of (7) into (6) gives the time-dependent density $n(\mathbf{X}, t)$. The perturbation theory is justified because the XUV pulse is weak. Stationary photoemission corresponds to $F(\omega) = \delta(\omega)$, cf. Eq. (14) of Ref. [30] and Eqs. (3.13)–(3.14) of Ref. [42]. Details of the derivation are presented in Appendix A.

Expression (7) is for a general case of a many-body system. For noninteracting electrons at $T = 0$ with a one-particle Hamiltonian $\hat{H}_0$, the explicit form of G_0^+ is

$$G_0^+(\mathbf{x}_1, \mathbf{x}_2, E) = 2i\pi \sum_{i \in \text{occ}} \psi_i(\mathbf{x}_1)\psi_i^*(\mathbf{x}_2)\delta(E - E_i), \tag{8}$$

where $\psi_i(\mathbf{x})$ are occupied eigenstates of $\hat{H}_0$: $\hat{H}_0\psi_i = E_i\psi_i$. Substituting Eq. (8) into Eq. (7) yields $G_2^+(\mathbf{X}, t, \mathbf{X}', t) = \sum_{i \in \text{occ}} \Psi_i(\mathbf{X}, t)\Psi_i^*(\mathbf{X}', t)$, where

$$\Psi_i(\mathbf{X}, t) \equiv \int \frac{d\epsilon}{2\pi} \int d^3\mathbf{x} G_0^r(\mathbf{X}, \mathbf{x}, \epsilon)\,\hat{o}(\mathbf{x}, \epsilon - \omega_X - E_i)\psi_i(\mathbf{x})$$

$$\times \exp(-i\epsilon t). \tag{9}$$

The function $\Psi_i(\mathbf{X}, t)$ has a clear physical meaning: It is the wave packet generated by the light pulse from the initial state $\psi_i(\mathbf{x})$. Equation (9) contains the same retarded GF as for a stationary photocurrent. Its asymptotics at $\mathbf{X} \to \infty$ is

$$G_0^r(\mathbf{X}, \mathbf{x}, \epsilon) \xrightarrow[\mathbf{X} \to \infty]{} -\frac{\exp(ikX)}{2\pi X}\Phi_\mathbf{k}(\mathbf{x}), \tag{10}$$

where $k \equiv \sqrt{2\epsilon}$, $\mathbf{k} = k\mathbf{X}/X$, and $\Phi_\mathbf{k}(\mathbf{x})$ is the LEED state [28,29,31,32], i.e., the scattering wave function for a plane wave incident *from* the detector at $\mathbf{X}$. Then the time-dependent density Eq. (6) at the detector is an incoherent sum of the densities of the wave packets of Eq. (9), $n(\mathbf{X}, t) = \sum_{i \in \text{occ}} |\Psi_i(\mathbf{X}, t)|^2$, where

$$\Psi_i(\mathbf{X}, t) = \frac{1}{X} \int d\epsilon \, \mathcal{A}_i(\mathbf{k}) \exp i[kX - \epsilon t + \eta_i(\mathbf{k})], \tag{11}$$

$$\mathcal{A}_i(\mathbf{k}) = \frac{1}{4\pi^2}F(\epsilon - \omega_X - E_i)|M_i(\mathbf{k})|, \tag{12}$$

$$M_i(\mathbf{k}) = \int d^3\mathbf{x} \, \Phi_\mathbf{k}(\mathbf{x})\hat{a}(\mathbf{x})\, \psi_i(\mathbf{x}), \tag{13}$$

where $\eta_i(\mathbf{k})$ is the phase of the matrix element $M_i(\mathbf{k}) = |M_i(\mathbf{k})|\exp i\eta_i(\mathbf{k})$. The maximum of the ith packet is situated at the stationary phase point $X = k(t - \tau_i)$ given by the condition $\partial[kX - \epsilon t + \eta_i(\mathbf{k})]/\partial\epsilon = 0$; the intercept time is given by the energy derivative

$$\tau_i = \partial\eta_i(\mathbf{k})/\partial\epsilon, \tag{14}$$

evaluated at the spectral peak of the packet $\mathcal{A}_i(\mathbf{k})$ Eq. (12).

The stationary phase formula is exact for narrow wave packets with peaked $\mathcal{A}_i(\mathbf{k})$. According to Eq. (12), the envelope $\mathcal{A}_i(\mathbf{k})$ is the envelope of the light pulse $F(\omega)$ (peaked at $\epsilon = \omega_X + E_i$) modulated by the matrix element $M_i(\mathbf{k})$. Thus, for an ultrashort pulse the function $\mathcal{A}_i(\mathbf{k})$ may be rather complex and have more than one maximum. Then τ must be calculated from the equation of motion for the expectation value $\langle \mathbf{X} \rangle$ of the position operator [18,43], see Appendix B.

Although the result Eq. (14) has the expected form of the EWS delay [16–18] its interpretation is not fully intuitive. The key quantity is the matrix element $M_i(\mathbf{k})$ between the initial state and the time-reversed LEED state $\Phi_\mathbf{k}^*$. First, the function $\Phi_\mathbf{k}^*$ in vacuum, apart from the wave going towards the detector contains beams incident onto the surface, including nonspecular beams due to lateral umklapp scattering. Second, inside the solid, $\Phi_\mathbf{k}^*$ contains only the waves propagating towards the surface while the true final state Ψ_i of Eq. (9) propagates in all directions.

III. RESULTS AND DISCUSSION

First we apply the one-step-EWS (OSTEWS) method to a finite 1D Kronig-Penney crystal: a 96-a.u.-long chain of 24 potential wells with a jellium substrate appended on the
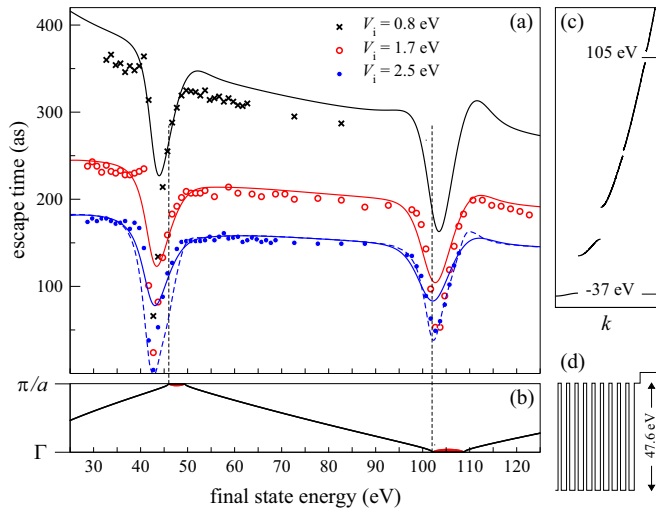
FIG. 1. (a) Photoelectron escape time versus final state energy for the Kronig-Penney crystal of Ref. [22] for $V_i = 0.8$, 1.7, and 2.5 eV. TDSE results (symbols) are compared with $\tau(E)$ by Eq. (14) (lines). Solid lines show $\tau(E)$ broadened according to the spectral width of the XUV pulse, and dashed line is the original curve for $V_i = 2.5$ eV. Vertical dashed lines show band maxima. (b), (c) Band structure $E(k)$. (d) Sketch of the crystal potential, see Ref. [22] for details.

left and vacuum on the right [19,22], Fig. 1(d). Photoelectrons are excited from the narrow band at −37.3 eV, and the intercept is averaged over the entire band. Figure 1(a) compares the escape time τ by Eq. (14) to the numerically exact TDSE result [22] obtained from simulated streaking spectrograms. In Ref. [22], inelastic scattering was included as a microscopic stochastic potential, and V_i was derived from the attenuation length. The OSTEWS curve is a convolution with an intensity-weighted Gaussian of 6 eV FWHM, which is the spectral width of the XUV pulse of 500 as FWHM duration [22].

The OSTEWS theory is seen to very closely agree with the full streaking TDSE calculations both in the nearly free-electron (NFE) region (between 50 and 95 eV final energy) and around the spectral gaps (at 47 and 105 eV). Well reproduced is the counterintuitive decrease of the escape time below the gaps, which was thoroughly discussed in Ref. [22]. At the minima, the dips are sharper in the TDSE streaking calculation than in OSTEWS, which underestimates their depths by about 50%. We ascribe this discrepancy to the interference effects in the ultrashort excitation, which in the vicinity of the spectral gaps lead to a complicated shape of the outgoing packet (both spatially and spectrally [22]). As a consequence, it propagates differently from the incoherent weighted sum of spectrally narrow packets. Interestingly, the OSTEWS τ values without the final-energy broadening yield the dip amplitudes in good agreement with the TDSE ones (dashed line in Fig. 1). In the NFE region, OSTEWS overestimates τ by about 6% for $V_i = 0.8$ eV, but the difference rapidly decreases in coming to larger (and more realistic) values of V_i. This slight difference is apparently due to the spatial aspect of streaking by a screened field: The packet becomes exposed to the laser field before it has completely left the crystal, its

spatial extent being the larger the larger is the photoelectron MFP (the smaller the V_i). Nevertheless, the neglect of the specific streaking mechanism in the OSTEWS theory does not significantly modify the τ curves, and the two theories are consistent in how they render the band-structure effects.

We now apply Eqs. (13) and (14) to photoemission from the real Mg(0001) surface. Magnesium is free-electron-like at low energies, so the laser field is efficiently screened [44], which simplifies the physics of the streaking experiment [2,7]. Here, both initial and final states are eigenfunctions of a density-functional Hamiltonian [in local density approximation (LDA)] with a realistic potential both in the bulk and at the surface, including the Z/r singularity at the nuclei. The LEED states are calculated with the embedding technique of Ref. [45] using the extended linear augmented plane waves method [46]. The calculations are fully *ab initio* save for the energy dependence of the optical potential, which is assumed to be a linear function $V_i(E) = 0.04E$. This closely approximates the $V_i(E)$ function for Al(111) derived from a measurement of stationary photoemission [47]. In calculating excitation energies, for the $2p$ binding energy we adopted the experimental value 50 eV [2] (the LDA result 42.6 eV is strongly underestimated). No correction is introduced for the valence band (VB). The calculations agree well with the measurements of stationary photoemission [7,48], in particular, regarding the energy dependence of the emission intensity from the surface state $I_{ss}(E)$, see Fig. 2(a).

The derivative of the photoelectron phase Eq. (14) averaged over the $2p$ band τ_{2p} and over the VB τ_{VB} are presented in Fig. 2(a) with circles accompanied by shading, whose vertical extent $\delta\tau$ shows the sensitivity of τ to a variation of V_i by ±10%, $\delta\tau = 0.1 \times V_i \, d\tau/dV_i$. The origin of the reference frame is 2.6 a.u. away from the outermost atomic layer, at the edge of the electronic density at the Mg(0001) surface. The $\tau(E)$ curves are a convolution with the intensity-weighted Gaussian of 4.2 eV FWHM. Crosses show the semiclassical NFE result $\tau_{NFE}(E) = 1/[2V_i(E)]$, for a photoelectron escaping from a depth equal to its MFP [1], with MFP being velocity times lifetime $1/2V_i$ [22].

The OSTEWS curves for the atomiclike $2p$ band and free-electron-like VB are seen to roughly follow $\tau_{NFE}(E)$ on a large scale, but locally both τ_{2p} and τ_{VB} strongly deviate from $\tau_{NFE}(E)$ over the whole range of 150 eV, showing reach structure caused by the lattice scattering. The underlying conducting complex band structure (CBS) Re $k_\perp(E)$ is presented in Fig. 2(b) as a decomposition of LEED states into partial waves (with complex Bloch vectors). To clearly reveal the connection to bulk bands, we used an abrupt surface barrier [49] and a negligible $V_i = 0.1$ eV. Most notably, there is no obvious relation between the escape time and the character of the final state: Indeed, the structures in the τ_{2p} and τ_{VB} curves are completely uncorrelated. Furthermore, the escape time from the surface state does not show any characteristic behavior: Neither the sharp intensity maximum at $E = 40$ eV nor the broad one at 127 eV correspond to an extremum of τ_{VB}. At the same time, both the narrow $2p$ band and the wide VB manifest rapid variations of τ, and it is the deep minimum at 74–80 eV in the $\tau_{2p}(E)$ curve that is responsible for the minimum of the delay curve $\Delta\tau(\omega) = \tau_{2p}(\omega) - \tau_{VB}(\omega)$ at around $\hbar\omega = 129$ eV in Fig. 2(c). We suggest this as the
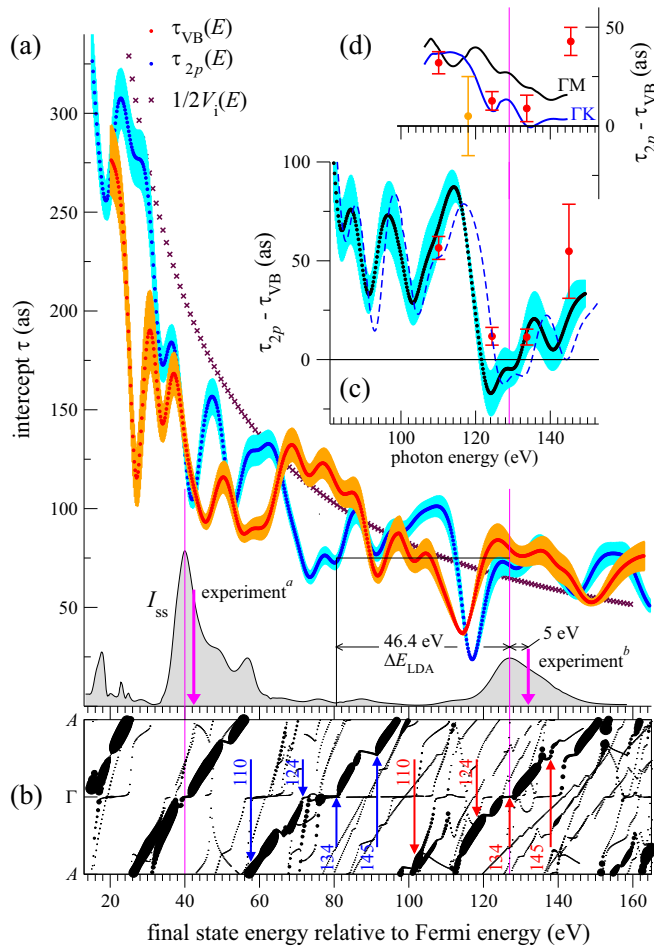
FIG. 2. (a) Escape time versus final state energy for normal emission from Mg(0001): blue shading for τ_{2p} and orange for $\tau_{\rm VB}$. Vertical extent of shading shows $\delta\tau = 0.1 \times V_i \, d\tau/dV_i$. Crosses are the function $1/[2V_i(E)]$. (b) Conducting CBS for $\mathbf{k}_\parallel = 0$. Size of the circle is proportional to the current carried by the Bloch wave at a given E and $k_\perp$. Final energies of the four measured excitations are shown by blue (2p) and red (VB) arrows. The numbers indicate the photon energies (self-energy correction is taken into account). (c) Delay $\tau_{2p} - \tau_{\rm VB}$ for $\mathbf{k}_\parallel = 0$: circles are the LDA calculation, shading shows $\delta\tau_{2p} + \delta\tau_{\rm VB}$. Dashed curve is the self-energy-corrected result. Red circles are the measurement of Ref. [7]. (d) θ-averaged delay (LDA) along $\bar{\Gamma}\bar{M}$ (black) and $\bar{\Gamma}\bar{K}$ (blue). Measurements are red circles [7] and the orange circle [2]. Black filled curve in graph (a) is the surface-state intensity $I_{\rm ss}(E)$. Vertical arrows indicate the $I_{\rm ss}(E)$ maxima measured in Ref. [48][a] and Ref. [7][b].

explanation of the experimentally observed drop of $\Delta\tau$ at 124.4 and 133.7 eV [7], see Fig. 2(c).

Unoccupied LDA eigenstates are known to have somewhat lower energies than the respective true quasiparticles. In particular, the measured surface-state intensity peaks at $\hbar\omega = 44$ eV [48] and at 134 eV [7] occur, respectively, 2 and 5 eV higher than in our calculation, Fig. 2(a). [A very similar energy dependence of the self-energy shift was observed for Al(111) [47].] A correction $E \to 1.039E$ brings the $I_{\rm ss}(E)$ peaks to the measured positions and yields the dashed $\Delta\tau$ curve in Fig. 2(c), which is in reasonable quantitative agreement with the experiment [7] except for the point at $\hbar\omega_{\rm X} =$

145 eV. Figure 2(d) compares angular-integrated measurements with the theoretical $\Delta\tau$ averaged over the experimental polar angle θ aperture of $22°$ for two azimuths, $\bar{\Gamma}\bar{M}$ and $\bar{\Gamma}\bar{K}$. We observe a substantial θ dependence of τ: the maximum deviation from the average is 30–40 as (depending on initial states and on azimuth), and the root mean square deviation is around 15 as. After the θ averaging, there remains an appreciable azimuthal dependence, Fig. 2(d). Averaged values show a much smoother $\hbar\omega$ dependence than the normal emission, in accord with the experiment. Finally, we comment on the conspicuous discrepancy at 145 eV. We tentatively ascribe it to the fact that the phase shift of the streaking spectrogram may not exactly coincide with the escape delay $\Delta\tau$. The latter implies that τ is measured when the packet has completely left the surface, whereas the actual streaking takes place right at the surface. We have seen similar discrepancy between TDSE and OSTEWS in Fig. 1: it is small in the NFE region but becomes large close to a gap. For Mg(0001), the final states of the four measured excitations are indicated by arrows in Fig. 2(b). Note that the 145 eV photons excite the VB electrons into a wide spectral gap, while the 2p electrons land at the bottom of a propagating branch. At the same time, for $\hbar\omega_{\rm X} = 110$ eV both final states are at the propagating branches, which may be the reason why $\tau_{\rm VB}$ underestimates the streaking measurement for $\hbar\omega_{\rm X} = 145$ eV, while for 110 eV the agreement with the experiment is rather good.

To summarize, we have developed an *ab initio* method for calculating the photoelectron escape time. In a one-step manner, the excitation and the scattering on the way out of the crystal are subsumed by the matrix element Eq. (13). The only parameters that we cannot calculate microscopically are the real and imaginary self-energy, but they were inferred from independent experiments, so adjustable parameters were avoided. According to our theory, in Mg(0001) the lattice-scattering-induced oscillations in the $\tau(\omega)$ curve greatly exceed the overall slow decrease due to the increasing inelastic scattering rate and persist up to kinetic energies above 150 eV. Their sharp and irregular shape is a consequence of the strong surface umklapp scattering and the multi-Bloch-wave composition of the Φ states. The streaking phase shift may deviate from the EWS escape delay because the latter ignores the details of the streaking at the surface. Nevertheless, the band structure effects are consistently reflected in the streaking experiment.

APPENDIX A: ONE-STEP FORMALISM FOR WAVE PACKETS

1. General formalism

Consider a semi-infinite crystal exposed to a time-dependent perturbation $\hat{O}$. The Dyson equation for the

Keldysh contour-ordered GF reads [30,40,41]

$$G(\mathbf{x}, t, \mathbf{x}', t') = G_0(\mathbf{x}, t, \mathbf{x}', t') + \int d^3\mathbf{x}_2 \int_C dt_2 G_0(\mathbf{x}, t, \mathbf{x}_2, t_2)\hat{O}(\mathbf{x}_2, t_2)G(\mathbf{x}_2, t_2, \mathbf{x}', t'), \tag{A1}$$

$$= G_0 + \int_C G_0\hat{O}G_0 + \int_C \int_C G_0\hat{O}G_0\hat{O}G_0 + \int_C \int_C \int_C G_0\hat{O}G_0\hat{O}G_0\hat{O}G, \tag{A2}$$

$$\equiv G_0 + G_1 + G_2 + \cdots, \tag{A3}$$

where T_C indicates ordering along the contour C going from $-\infty$, passing the points t and t', and then returning back to $-\infty$ [40]. The function G_0 is the equilibrium GF of the system in the absence of radiation. Equation (A2) uses the compact notations $G(\mathbf{x}_1, t_1, \mathbf{x}_2, t_2) \equiv G(1, 2)$, etc.; and

$$\int_C AB \equiv \int d^3\mathbf{x}_2 \int_C dt_2 A(1, 2)B(2, 3).$$

In the following, we will denote

$$AB \equiv \int d^3\mathbf{x}_2 \int_{-\infty}^{+\infty} dt_2 A(1, 2)B(2, 3).$$

The crystal occupies the half-space $x < 0$, and the electrons photoexcited above the vacuum level are detected at a point $\mathbf{X}$ at a large distance from the crystal surface. The radial photocurrent $j(\mathbf{X}, t)$ of electrons emitted from the target along the observation direction is given by [30]

$$j(\mathbf{X}, t) = \lim_{\substack{\mathbf{X}' \to \mathbf{X}, \\ \mathbf{X} \to \infty}} \left(\frac{\partial}{\partial X'} - \frac{\partial}{\partial X} \right) G_2^+(\mathbf{X}, t, \mathbf{X}', t). \tag{A4}$$

The light pulse creates a superposition of wave packets, whose density evolution, Eq. (6), is found from the same "lesser" GF Eq. (2). Subscript 2 means the second order of the perturbation theory with respect to $\hat{O}(\mathbf{x}, t)$, i.e.,

$$G_2^+(\mathbf{X}, t, \mathbf{X}', t') = \left[\int_C \int_C G_0\hat{O}G_0\hat{O}G_0 \right]^+ = G_0^r\hat{O}G_0^r\hat{O}G_0^+ + G_0^r\hat{O}G_0^+\hat{O}G_0^a + G_0^+\hat{O}G_0^a\hat{O}G_0^a, \tag{A5}$$

where we have introduced the retarded and advanced GFs,

$$G^r(\mathbf{x}, t, \mathbf{x}', t') = -i\theta(t - t')\langle\{\hat{\psi}(\mathbf{x}, t), \hat{\psi}^\dagger(\mathbf{x}', t')\}\rangle, \tag{A6}$$

$$G^a(\mathbf{x}, t, \mathbf{x}', t') = i\theta(t' - t)\langle\{\hat{\psi}(\mathbf{x}, t), \hat{\psi}^\dagger(\mathbf{x}', t')\}\rangle, \tag{A7}$$

with $\{\hat{A}, \hat{B}\} \equiv \hat{A}\hat{B} + \hat{B}\hat{A}$ and $\theta(t) \equiv (t/|t| + 1)/2$ being the step function. In Eq. (A5), we have used the Langreth theorem [41,42,50]:

$$\left[\int_C dt_2 A(t, t_2)B(t_2, t') \right]^+ = \int_{-\infty}^{+\infty} dt_2 [A^r(t, t_2)B^+(t_2, t') + A^+(t, t_2)B^a(t_2, t')], \tag{A8}$$

$$\left[\int_C dt_2 A(t, t_2)B(t_2, t') \right]^s = \int_{-\infty}^{+\infty} dt_2 A^s(t, t_2)B^s(t_2, t'), \quad s = r, a. \tag{A9}$$

In the explicit form, Eq. (A5) reads

$$G_2^+(\mathbf{X}, t, \mathbf{X}', t') = \int_{-\infty}^{+\infty} dt_2 \int d^3\mathbf{x}_2 \int_{-\infty}^{+\infty} dt_3 \int d^3\mathbf{x}_3 \{ G_0^r(\mathbf{X}, t, \mathbf{x}_2, t_2)\hat{O}(\mathbf{x}_2, t_2)G_0^r(\mathbf{x}_2, t_2, \mathbf{x}_3, t_3)\hat{O}(\mathbf{x}_3, t_3)G_0^+(\mathbf{x}_3, t_3, \mathbf{X}', t')$$

$$+ G_0^r(\mathbf{X}, t, \mathbf{x}_2, t_2)\hat{O}(\mathbf{x}_2, t_2)G_0^+(\mathbf{x}_2, t_2, \mathbf{x}_3, t_3)\hat{O}(\mathbf{x}_3, t_3)G_0^a(\mathbf{x}_3, t_3, \mathbf{X}', t')$$

$$+ G_0^+(\mathbf{X}, t, \mathbf{x}_2, t_2)\hat{O}(\mathbf{x}_2, t_2)G_0^a(\mathbf{x}_2, t_2, \mathbf{x}_3, t_3)\hat{O}(\mathbf{x}_3, t_3)G_0^a(\mathbf{x}_3, t_3, \mathbf{X}', t') \}. \tag{A10}$$

Note that the time integration on the right-hand side is over the real axis.

The equilibrium GFs G_0^s with $s = +, -, a, r$ depend only on difference of their time arguments and may be expressed via Fourier transforms:

$$G_0^s(t - t') = \frac{1}{2\pi} \int_{-\infty}^{+\infty} G_0^s(\omega)e^{-i\omega(t-t')}d\omega, \tag{A11}$$

$$G_0^s(\omega) = \int_{-\infty}^{+\infty} G_0^s(t)e^{i\omega t}dt. \tag{A12}$$

Substitution of expression (A11) into Eq. (A10) gives

$$
\begin{aligned}
G_2^+(\mathbf{X}, t, \mathbf{X}', t') = \iint d^3\mathbf{x}_2 d^3\mathbf{x}_3 &\iiint \frac{d\epsilon dE d\epsilon'}{8\pi^3} \exp(-i\epsilon t + i\epsilon' t') \\
&\times \big[G_0^r(\mathbf{X}, \mathbf{x}_2, \epsilon) \hat{O}(\mathbf{x}_2, \epsilon - E) G_0^r(\mathbf{x}_2, \mathbf{x}_3, E) \hat{O}(\mathbf{x}_3, E - \epsilon') G_0^+(\mathbf{x}_3, \mathbf{X}', \epsilon') \\
&+ G_0^r(\mathbf{X}, \mathbf{x}_2, \epsilon) \hat{O}(\mathbf{x}_2, \epsilon - E) G_0^+(\mathbf{x}_2, \mathbf{x}_3, E) \hat{O}(\mathbf{x}_3, E - \epsilon') G_0^a(\mathbf{x}_3, \mathbf{X}', \epsilon') \\
&+ G_0^+(\mathbf{X}, \mathbf{x}_2, \epsilon) \hat{O}(\mathbf{x}_2, \epsilon - E) G_0^a(\mathbf{x}_2, \mathbf{x}_3, E) \hat{O}(\mathbf{x}_3, E - \epsilon') G_0^a(\mathbf{x}_3, \mathbf{X}', \epsilon') \big],
\end{aligned}
\tag{A13}
$$

where

$$
\hat{O}(\mathbf{x}, \omega) = \hat{a}(\mathbf{x})\alpha(\omega), \text{ and } \alpha(\omega) = \int_{-\infty}^{+\infty} F(t)\cos(\omega_\mathrm{x} t)\exp(i\omega t)\, dt = F(\omega + \omega_\mathrm{x}) + F(\omega - \omega_\mathrm{x}).
\tag{A14}
$$

The envelope function $F(t)$ vanishes outside a subfemtosecond interval, before which the crystal is at equilibrium. It is convenient to assume $F(t) = F(-t)$, so it is $F(\omega) = F(-\omega)$. The "lesser" function describes occupied electron states [30,40]

$$
G_0^+(\mathbf{x}_1, \mathbf{x}_2, E) = -2if(E - E_\mathrm{F})\mathrm{Im}\, G_0^r(\mathbf{x}_1, \mathbf{x}_2, E),
\tag{A15}
$$

where $f(E) = 1/[\exp(\beta E) + 1]$ is the Fermi distribution function, which deviates from $\theta(-E)$ in an energy interval $\Delta E \sim 1/\beta \ll |E_\mathrm{F}|$, where $E_\mathrm{F} = -W$ is the Fermi energy and W is the work function of the solid. The energy is relative to the vacuum level. The electrons are confined within the crystal, hence, we have for the "lesser" functions:

$$
G_0^+(\mathbf{X} \to \infty, \mathbf{x}, E) = G_0^+(\mathbf{x}, \mathbf{X}' \to \infty, E) = 0 \text{ for } E > 0.
$$

So, only the second term is nonzero on the right-hand side of Eq. (A13):

$$
\begin{aligned}
G_2^+(\mathbf{X}, t, \mathbf{X}', t') = \iint d^3\mathbf{x}_2 d^3\mathbf{x}_3 &\iiint \frac{d\epsilon dE d\epsilon'}{8\pi^3} \exp(-i\epsilon t + i\epsilon' t') \\
&\times G_0^r(\mathbf{X}, \mathbf{x}_2, \epsilon) \hat{O}(\mathbf{x}_2, \epsilon - E) G_0^+(\mathbf{x}_2, \mathbf{x}_3, E) \hat{O}(\mathbf{x}_3, E - \epsilon') G_0^a(\mathbf{x}_3, \mathbf{X}', \epsilon').
\end{aligned}
\tag{A16}
$$

For a while, we will use the shorthand notations and drop the spatial variables. We substitute

$$
\hat{O}(\omega) = \hat{o}(\omega + \omega_\mathrm{x}) + \hat{o}(\omega - \omega_\mathrm{x})
\tag{A17}
$$

into Eq. (A16) and obtain

$$
\begin{aligned}
G_2^+(t, t) &= \iiint \frac{d\epsilon dE d\epsilon'}{8\pi^3} \exp[-i(\epsilon - \epsilon')t] G_0^r(\epsilon)[\hat{o}(\epsilon - E + \omega_\mathrm{x}) + \hat{o}(\epsilon - E - \omega_\mathrm{x})]G_0^+(E) \\
&\quad \times [\hat{o}(E - \epsilon' + \omega_\mathrm{x}) + \hat{o}(E - \epsilon' - \omega_\mathrm{x})]G_0^a(\epsilon') \\
&= \iiint \frac{d\epsilon dE d\epsilon'}{8\pi^3} \exp[-i(\epsilon - \epsilon')t] G_0^r(\epsilon)[\hat{o}(\epsilon - E + \omega_\mathrm{x})G_0^+(E)\hat{o}(E - \epsilon' + \omega_\mathrm{x}) + \hat{o}(\epsilon - E + \omega_\mathrm{x})G_0^+(E) \\
&\quad \times \hat{o}(E - \epsilon' - \omega_\mathrm{x}) + \hat{o}(\epsilon - E - \omega_\mathrm{x})G_0^+(E)\hat{o}(E - \epsilon' + \omega_\mathrm{x}) + \hat{o}(\epsilon - E - \omega_\mathrm{x})G_0^+(E)\hat{o}(E - \epsilon' - \omega_\mathrm{x})]G_0^a(\epsilon').
\end{aligned}
\tag{A18}
$$

In Eqs. (A18), the integration is only over positive ϵ and ϵ', because only electrons with energies higher than the vacuum level can escape from the target:

$$
G_0^r(\mathbf{X} \to \infty, \mathbf{x}, \epsilon) = G_0^a(\mathbf{x}, \mathbf{X}' \to \infty, \epsilon') = 0 \text{ for } \epsilon < 0.
$$

Now we note that for sufficiently long duration D_x of the XUV pulse, the Fourier transform of the envelope function $F(\omega)$ has a sharp maximum at $\omega = 0$ [$F(\omega) = \delta(\omega)$ for a stationary photoemission], and its width estimated from the uncertainty relation $\Delta\omega \sim 1/2D_\mathrm{x}$ is several eV. Thus, in the first two terms of Eq. (A18), the integration over E is, in fact, restricted to the interval $\epsilon + \omega_\mathrm{x} - 1/2D_\mathrm{x} < E < \epsilon + \omega_\mathrm{x} + 1/2D_\mathrm{x}$. The XUV photon energy ω_x is of the order of 100 eV, so the argument E of the "lesser" function in the two terms is well above the Fermi energy, $E > \epsilon + \omega_\mathrm{x} - 1/2D_\mathrm{x} > 0 > E_F$, so this function vanishes (cf. the analysis of Eq. (13) in Ref. [30]). The fourth term vanishes because $E > \epsilon' + \omega_\mathrm{x} - 1/2D_\mathrm{x} > 0 > E_F$. Thus, only the third term in Eq. (A18) survives.

Restoring the explicit notation for the arguments of all functions we arrive at Eq. (7).

The substitution of expression Eq. (7) into Eqs. (6) and (A4) gives the time-dependent probability density and the *total* photocurrent. The stationary case corresponds to $F(\omega) = \delta(\omega)$ [cf. expression Eq. (14) for the photocurrent in Ref. [30], and see also Eqs. (3.13) and (3.14) in Ref. [42]]. Note that the derivation of Eq. (7) from Eq. (A5) holds for the general case of a many-body Hamiltonian $\hat{H}_0$ in Eq. (3).

2. Noninteracting electrons

For a non-interacting system, the explicit form for G_0^+ is

$$
G_0^+(\mathbf{x}_1, \mathbf{x}_2, E) = 2if(E - E_\mathrm{F})\pi \sum_i \psi_i(\mathbf{x}_1)\psi_i^*(\mathbf{x}_2)\delta(E - E_i).
\tag{A19}
$$

We substitute Eq. (A19) into Eq. (7) to obtain

$$
G_2^+(\mathbf{X}, t, \mathbf{X}', t)
$$

$$
= 2i\pi \sum_i f(E_i - E_F) \iiint \frac{d\epsilon \, d\epsilon' dE}{8\pi^3}
$$

$$
\times \int d^3\mathbf{x}_2 \, G_0^r(\mathbf{X}, \mathbf{x}_2, \epsilon) \hat{o}(\mathbf{x}_2, \epsilon - \omega_X - E) \psi_i(\mathbf{x}_2)
$$

$$
\times \int d^3\mathbf{x}_3 \, \psi_i^*(\mathbf{x}_3) \hat{o}(\mathbf{x}_3, E + \omega_X - \epsilon') G_0^a(\mathbf{x}_3, \mathbf{X}', \epsilon')
$$

$$
\times \delta(E - E_i) \exp{-i(\epsilon' + E)t},
$$

which in terms of the final states $\Psi_i(\mathbf{X}, t)$ given by Eq. (9) reads

$$
G_2^+(\mathbf{X}, t, \mathbf{X}', t) = i \sum_i f(E_i - E_F) \Psi_i(\mathbf{X}, t) \Psi_i^*(\mathbf{X}', t).
$$

$$
\text{(A20)}
$$

Now, following Ref. [28], we use the Dyson identity

$$
G_0^r(\mathbf{X}, \mathbf{x}, \epsilon)
$$

$$
= g(\mathbf{X} - \mathbf{x}, \epsilon) + \int d^n\mathbf{x}' \, g(\mathbf{X} - \mathbf{x}', \epsilon) V(\mathbf{x}') G_0^r(\mathbf{x}', \mathbf{x}, \epsilon),
$$

$$
\text{(A21)}
$$

into which we now substitute the free particle GF for asymptotically large X and finite $\mathbf{x}$ for the n-dimensional space:

$$
g(\mathbf{X} - \mathbf{x}, \epsilon) = \frac{1}{ik} \left(\frac{-ik}{2\pi X} \right)^{(n-1)/2} \exp[\, ikX - i\mathbf{k}\mathbf{x} \,], \quad \text{where}
$$

$$
k \equiv \sqrt{2\epsilon} \quad \text{and} \quad \mathbf{k} = k\mathbf{X}/X. \quad \text{(A22)}
$$

This leads to the asymptotic expression (10) for $G_0^r(\mathbf{X}, \mathbf{x}_2, \epsilon)$ as $\mathbf{X} \to \infty$, which yields the density and the photocurrent in terms of the LEED states:

$$
\Phi_\mathbf{k}(\mathbf{x}) = e^{-i\mathbf{k}\mathbf{x}} + \int d^3\mathbf{x}' e^{-i\mathbf{k}\mathbf{x}'} V(\mathbf{x}') G_0^r(\mathbf{x}', \mathbf{x}, \epsilon). \quad \text{(A23)}
$$

By substituting the asymptotic form Eq. (10) of $G_0^r(\mathbf{X}, \mathbf{x}, \omega)$ into Eq. (9), we obtain the expressions Eqs. (11)–(13) for the true final state $\Psi_i(\mathbf{X}, t)$.

APPENDIX B: TIME DELAY IN PHOTOEMISSION

It follows from Eqs. (6) and (A20) that the density in vacuum reduces to an incoherent superposition of wave packets generated by the light pulse from the initial states

$$
n(\mathbf{X}, t) = \sum_i f(E_i - E_F) |\Psi_i(\mathbf{X}, t)|^2. \quad \text{(B1)}
$$

For a spectrally very narrow wave packet with $\mathcal{A}_i(\mathbf{k})$, Eq. (12), sharply peaked around some energy ϵ_0, the maximum of the packet at a time t is situated at the stationary phase point X given by the condition Eq. (14). For an ultrashort pulse, the realistic function $\mathcal{A}_i(\mathbf{k})$ may be rather complex, e.g., it may have several peaks. Then the average time delay should be found from the equation of motion for the position expectation value $\langle \mathbf{X} \rangle$.

Here we present a calculation of $\langle \mathbf{X} \rangle$ for a 1D system. The expression Eq. (A22) for $n = 1$ gives the 1D GF asymptotics

$$
G_0^r(X, x, \epsilon) \xrightarrow[X \to \infty]{} -\frac{i \exp[ikX]}{k} \Phi(x, k), \quad \text{(B2)}
$$

and the 1D LEED states are

$$
\Phi(x, k) = e^{-ikx} + \int dx' e^{-ikx'} V(x') G_0^r(x', x, \epsilon). \quad \text{(B3)}
$$

Instead of Eqs. (11)–(13), for a one-dimensional system we obtain

$$
\Psi_i(X, t) = \int d\epsilon \, \mathcal{A}_i(k) \exp i[kX - \epsilon t + \eta_i(k)], \quad \text{(B4)}
$$

$$
\mathcal{A}_i(k) = \frac{1}{2\pi} \frac{F(\epsilon - \omega_X - E_i)}{k} |M_i(k)|, \quad \text{(B5)}
$$

$$
M_i(k) = \int dx \, \Phi(x, k) \hat{a}(x) \psi_i(x) = |M_i(k)| \exp i\eta_i(k), \quad \text{(B6)}
$$

where $\eta_i(k)$ is the phase of matrix element $M_i(k)$.

Now we calculate the position expectation value

$$
\langle X \rangle = B \sum_{i \in \text{occ}} \int_{-\infty}^{\infty} X dX \int_0^{\infty} k' dk' \int_0^{\infty} k dk \, \mathcal{A}_i(k')
$$

$$
\times \exp[-i(k' - k)X] \mathcal{A}_i(k)
$$

$$
\times \exp\left\{ -i[\eta_i(k') - \eta_i(k)] + i\frac{k'^2 - k^2}{2}t \right\}, \quad \text{(B7)}
$$

where B is the normalization constant

$$
B = \left[2\pi \sum_{i \in \text{occ}} \int_0^{\infty} k^2 \mathcal{A}_i^2(k) dk \right]^{-1}. \quad \text{(B8)}
$$

In Eqs. (B7) and (B8), we have assumed that $f(E - E_F) \approx \theta(E_F - E)$. The integration over X in Eq. (B7) gives

$$
\int_{-\infty}^{\infty} X \exp[-i(k' - k)X] dX
$$

$$
= -i\frac{\partial}{\partial k} \int_{-\infty}^{\infty} \exp[-i(k' - k)X] dX = -2\pi i \frac{\partial}{\partial k} \delta(k - k').
$$

Finally, we obtain

$$
\langle X \rangle = 2\pi i B \sum_{i \in \text{occ}} \int_0^{\infty} k' \mathcal{A}_i(k') \exp\left[-i\eta_i(k') + i\frac{k'^2}{2}t \right]
$$

$$
\times \frac{\partial}{\partial k} \left\{ k\mathcal{A}_i(k) \exp\left[i\left(\eta_i(k) - \frac{k^2}{2}t \right) \right] \right\}_{k=k'} dk'
$$

$$
= 2\pi B \sum_{i \in \text{occ}} \int_0^{\infty} [k\mathcal{A}_i(k)]^2 k[t - \dot{\eta}_i(k)] \, dk \equiv \bar{k}t + b
$$

$$
\equiv \bar{k}(t - \bar{\tau}), \quad \text{(B9)}
$$

$$
\bar{k} \equiv 2\pi B \sum_{i \in \text{occ}} \int_0^{\infty} [k\mathcal{A}_i(k)]^2 k \, dk, \quad \text{(B10)}
$$

$$
b \equiv -2\pi B \sum_{i \in \text{occ}} \int_0^{\infty} [k\mathcal{A}_i(k)]^2 \tau_i(k) k \, dk, \quad \text{(B11)}
$$

$$
\bar{\tau} = -\frac{b}{\bar{k}}. \quad \text{(B12)}
$$

[1] A. L. Cavalieri, N. Mueller, T. Uphues, V. S. Yakovlev, A. Baltuska, B. Horvath, B. Schmidt, L. Bluemel, R. Holzwarth, S. Hendel, M. Drescher, U. Kleineberg, P. M. Echenique, R. Kienberger, F. Krausz, and U. Heinzmann, Attosecond spectroscopy in condensed matter, Nature **449**, 1029 (2007).

[2] S. Neppl, R. Ernstorfer, E. M. Bothschafter, A. L. Cavalieri, D. Menzel, J. V. Barth, F. Krausz, R. Kienberger, and P. Feulner, Attosecond Time-Resolved Photoemission from Core and Valence States of Magnesium, Phys. Rev. Lett. **109**, 087401 (2012).

[3] S. Neppl, R. Ernstorfer, A. L. Cavalieri, C. Lemell, G. Wachter, E. Magerl, E. M. Bothschafter, M. Jobst, M. Hofstetter, U. Kleineberg, J. V. Barth, D. Menzel, J. Burgdorfer, P. Feulner, F. Krausz, and R. Kienberger, Direct observation of electron propagation and dielectric screening on the atomic length scale, Nature **517**, 342 (2015).

[4] W. A. Okell, T. Witting, D. Fabris, C. A. Arrell, J. Hengster, S. Ibrahimkutty, A. Seiler, M. Barthelmess, S. Stankov, D. Y. Lei, Y. Sonnefraud, M. Rahmani, T. Uphues, S. A. Maier, J. P. Marangos, and J. W. G. Tisch, Temporal broadening of attosecond photoelectron wavepackets from solid surfaces, Optica **2**, 383 (2015).

[5] F. Siek, S. Neb, P. Bartz, M. Hensen, C. Strüber, S. Fiechter, M. Torrent-Sucarrat, V. Silkin, E. Krasovskii, N. Kabachnik, S. Fritzsche, R. Muiño, P. Echenique, A. Kazansky, N. Müller, W. Pfeiffer, and U. Heinzmann, Angular momentum-induced delays in solid-state photoemission enhanced by intra-atomic interactions, Science **357**, 1274 (2017).

[6] M. Ossiander, J. Riemensberger, S. Neppl, M. Mittermair, M. Schäffer, A. Duensing, M. S. Wagner, R. Heider, M. Wurzer, M. Gerl, M. Schnitzenbaumer, J. V. Barth, F. Libisch, C. Lemell, J. Burgdörfer, P. Feulner, and R. Kienberger, Absolute timing of the photoelectric effect, Nature **561**, 374 (2018).

[7] J. Riemensberger, S. Neppl, D. Potamianos, M. Schäffer, M. Schnitzenbaumer, M. Ossiander, C. Schröder, A. Guggenmos, U. Kleineberg, D. Menzel, F. Allegretti, J. V. Barth, R. Kienberger, P. Feulner, A. G. Borisov, P. M. Echenique, and A. K. Kazansky, Attosecond Dynamics of sp-Band Photoexcitation, Phys. Rev. Lett. **123**, 176801 (2019).

[8] R. Locher, L. Castiglioni, M. Lucchini, M. Greif, L. Gallmann, J. Osterwalder, M. Hengsberger, and U. Keller, Energy-dependent photoemission delays from noble metal surfaces by attosecond interferometry, Optica **2**, 405 (2015).

[9] Z. Tao, C. Chen, T. Szilvási, M. Keller, M. Mavrikakis, H. Kapteyn, and M. Murnane, Direct time-domain observation of attosecond final-state lifetimes in photoemission from solids, Science **353**, 62 (2016).

[10] L. Kasmi, M. Lucchini, L. Castiglioni, P. Kliuiev, J. Osterwalder, M. Hengsberger, L. Gallmann, P. Krüger, and U. Keller, Effective mass effect in attosecond electron transport, Optica **4**, 1492 (2017).

[11] A. K. Kazansky and P. M. Echenique, One-Electron Model for the Electronic Response of Metal Surfaces to Subfemtosecond Photoexcitation, Phys. Rev. Lett. **102**, 177401 (2009).

[12] C.-H. Zhang and U. Thumm, Streaking and Wigner time delays in photoemission from atoms and surfaces, Phys. Rev. A **84**, 033401 (2011).

[13] Q. Liao and U. Thumm, Attosecond time-resolved streaked photoemission from Mg-covered W(110) surfaces, Phys. Rev. A **92**, 031401(R) (2015).

[14] A. Gebauer, S. Neb, W. Enns, B. Stadtmüller, M. Aeschlimann, and W. Pfeiffer, Equivalence of RABBITT and streaking delays in attosecond-time-resolved photoemission spectroscopy at solid surfaces, Appl. Sci. **9**, 592 (2019).

[15] M. J. Ambrosio and U. Thumm, Spatiotemporal analysis of a final-state shape resonance in interferometric photoemission from Cu(111) surfaces, Phys. Rev. A **100**, 043412 (2019).

[16] M. Schultze, M. Fieß, N. Karpowicz, J. Gagnon, M. Korbman, M. Hofstetter, S. Neppl, A. L. Cavalieri, Y. Komninos, T. Mercouris, C. A. Nicolaides, R. Pazourek, S. Nagele, J. Feist, J. Burgdörfer, A. M. Azzeer, R. Ernstorfer, R. Kienberger, U. Kleineberg, E. Goulielmakis, F. Krausz, and V. S. Yakovlev, Delay in photoemission, Science **328**, 1658 (2010).

[17] A. S. Kheifets and I. A. Ivanov, Delay in Atomic Photoionization, Phys. Rev. Lett. **105**, 233002 (2010).

[18] R. Pazourek, S. Nagele, and J. Burgdörfer, Attosecond chronoscopy of photoemission, Rev. Mod. Phys. **87**, 765 (2015).

[19] E. E. Krasovskii, Attosecond spectroscopy of solids: Streaking phase shift due to lattice scattering, Phys. Rev. B **84**, 195106 (2011).

[20] A. G. Borisov, D. Sánchez-Portal, A. K. Kazansky, and P. M. Echenique, Resonant and nonresonant processes in attosecond streaking from metals, Phys. Rev. B **87**, 121110(R) (2013).

[21] Q. Liao and U. Thumm, Attosecond Time-Resolved Photoelectron Dispersion and Photoemission Time Delays, Phys. Rev. Lett. **112**, 023602 (2014).

[22] E. E. Krasovskii, C. Friedrich, W. Schattke, and P. M. Echenique, Rapid propagation of a Bloch wave packet excited by a femtosecond ultraviolet pulse, Phys. Rev. B **94**, 195434 (2016).

[23] Q. Liao, W. Cao, Q. Zhang, K. Liu, F. Wang, P. Lu, and U. Thumm, Distinction of Electron Dispersion in Time-Resolved Photoemission Spectroscopy, Phys. Rev. Lett. **125**, 043201 (2020).

[24] C. Lemell, B. Solleder, K. Tőkési, and J. Burgdörfer, Simulation of attosecond streaking of electrons emitted from a tungsten surface, Phys. Rev. A **79**, 062901 (2009).

[25] C. Lemell, S. Neppl, G. Wachter, K. Tőkési, R. Ernstorfer, P. Feulner, R. Kienberger, and J. Burgdörfer, Real-time observation of collective excitations in photoemission, Phys. Rev. B **91**, 241101(R) (2015).

[26] E. E. Krasovskii and W. Schattke, Angle-Resolved Photoemission from Surface States, Phys. Rev. Lett. **93**, 027601 (2004).

[27] E. E. Krasovskii, V. N. Strocov, N. Barrett, H. Berger, W. Schattke, and R. Claessen, Band mapping in the one-step photoemission theory: Multi-Bloch-wave structure of final states and interference effects, Phys. Rev. B **75**, 045432 (2007).

[28] I. Adawi, Theory of the surface photoelectric effect for one and two photons, Phys. Rev. **134**, A788 (1964).

[29] G. D. Mahan, Theory of photoemission in simple metals, Phys. Rev. B **2**, 4334 (1970).

[30] C. Caroli, D. Lederer-Rozenblatt, B. Roulet, and D. Saint-James, Inelastic effects in photoemission: Microscopic formulation and qualitative discussion, Phys. Rev. B **8**, 4552 (1973).

[31] P. J. Feibelman and D. E. Eastman, Photoemission spectroscopy—correspondence between quantum theory and experimental phenomenology, Phys. Rev. B **10**, 4932 (1974).

[32] R. O. Kuzian and E. E. Krasovskii, One-step approach to ARPES from strongly correlated solids: A Mott − Hubbard system, Phys. Rev. B **94**, 115119 (2016).

[33] J. Pendry, Theory of photoemission, Surf. Sci. **57**, 679 (1976).

[34] J. Braun, The theory of angle-resolved ultraviolet photoemission and its applications to ordered materials, Rep. Prog. Phys. **59**, 1267 (1996).

[35] L. Eisenbud, The formal properties of nuclear collisions, Ph.D. thesis, Princeton University, 1948.

[36] E. P. Wigner, Lower limit for the energy derivative of the scattering phase shift, Phys. Rev. **98**, 145 (1955).

[37] F. T. Smith, Lifetime matrix in collision theory, Phys. Rev. **118**, 349 (1960).

[38] J. K. Freericks, H. R. Krishnamurthy, and T. Pruschke, Theoretical Description of Time-Resolved Photoemission Spectroscopy: Application to Pump-Probe Experiments, Phys. Rev. Lett. **102**, 136401 (2009).

[39] J. Braun, R. Rausch, M. Potthoff, J. Minár, and H. Ebert, One-step theory of pump-probe photoemission, Phys. Rev. B **91**, 035119 (2015).

[40] L. V. Keldysh, Diagram technique for nonequilibrium processes, J. Exptl. Theoret. Phys. (U.S.S.R.) **47**, 1515 (1964) [Sov. Phys. JETP **20**, 1018 (1965)].

[41] H. Haug and A.-P. Jauho, Contour-ordered Green functions, in *Quantum Kinetics in Transport and Optics of Semiconductors*, edited by M. Cardona, P. Fulde, K. von Klitzing, R. Merlin, H.-J. Queisser, and H. Störmer (Springer, Berlin, 2008), pp. 63–73.

[42] D. C. Langreth, Linear and nonlinear response theory with applications, in *Linear and Nonlinear Electron Transport in Solids*, edited by J. T. Devreese and V. E. van Doren (Springer US, Boston, MA, 1976), pp. 3–32.

[43] C. de Carvalho and H. Nussenzveig, Time delay, Phys. Rep. **364**, 83 (2002).

[44] E. E. Krasovskii, V. M. Silkin, V. U. Nazarov, P. M. Echenique, and E. V. Chulkov, Dielectric screening and band-structure effects in low-energy photoemission, Phys. Rev. B **82**, 125102 (2010).

[45] E. E. Krasovskii, Augmented-plane-wave approach to scattering of Bloch electrons by an interface, Phys. Rev. B **70**, 245322 (2004).

[46] E. E. Krasovskii, Accuracy and convergence properties of the extended linear augmented-plane-wave method, Phys. Rev. B **56**, 12866 (1997).

[47] E. E. Krasovskii, W. Schattke, P. Jiříček, M. Vondráček, O. V. Krasovska, V. N. Antonov, A. P. Shpak, and I. Bartoš, Photoemission from Al(100) and (111): Experiment and ab initio theory, Phys. Rev. B **78**, 165406 (2008).

[48] R. A. Bartynski, R. H. Gaylord, T. Gustafsson, and E. W. Plummer, Angle-resolved photoemission study of the surface and bulk electronic structure of Mg(0001) and Mg(1120), Phys. Rev. B **33**, 3644 (1986).

[49] E. E. Krasovskii and W. Schattke, Calculation of the wave functions for semi-infinite crystals with linear methods of band theory, Phys. Rev. B **59**, R15609(R) (1999).

[50] D. C. Langreth and J. W. Wilkins, Theory of spin resonance in dilute magnetic alloys, Phys. Rev. B **6**, 3189 (1972).